NANOSYSTEMS:
PHYSICS, CHEMISTRY, MATHEMATICS

Original article

Kovalevskaya K.S., et al. *Nanosystems: Phys. Chem. Math.*, 2025, **16** (6), 872–886.
http://nanojournal.ifmo.ru
DOI 10.17586/2220-8054-2025-16-6-872-886

The relationship between the impregnation solution composition and the active component distribution NiMo/ZSM-23 catalysts for the plant lipids hydroprocessing

Ksenia S. Kovalevskaya, Roman G. Kukushkin, Olesya O. Zaikina, Olga A. Bulavchenko, Vadim A. Yakovlev

Boreskov Institute of Catalysis SB RAS, Novosibirsk, Russia

Corresponding author: Roman G. Kukushkin, roman@catalysis.ru

ABSTRACT The nature of the interaction between metals and a catalyst support is a crucial factor in determining the dispersed state of active component phases. In this study, a series of Ni-Mo/ZSM-23 catalysts for the hydroprocessing of plant lipids was prepared by incipient wetness impregnation. The catalysts were prepared by a different sequence of metal deposition and using various complexing agents. The catalysts were investigated by a few physico-chemical methods (TPR, UV-Vis spectroscopy, XRD, TPD-NH_3, Raman spectroscopy, HRTEM). It was found that the charge of the ZSM-23 zeolite surface (positive/negative) and the type of metal ions in the impregnation solution affect the formation of phases on the support surface. The use of ammonia impregnating solutions leads to the formation of phases NiO, α-$NiMoO_4$ and β-$NiMoO_4$. In the case of using aqueous and citrate impregnating solutions, only the formation of NiO and β-$NiMoO_4$ phases is observed.

KEYWORDS nickel, molybdenum, ZSM-23, impregnating solutions, PZC

ACKNOWLEDGEMENTS This work was supported by the Ministry of Science and Higher Education of the Russian Federation within the governmental assignment for Boreskov Institute of Catalysis (project(s) FWUR-2024-0038).

FOR CITATION Kovalevskaya K.S., Kukushkin R.G., Zaikina O.O., Bulavchenko O.A., Yakovlev V.A. The relationship between the impregnation solution composition and the active component distribution NiMo/ZSM-23 catalysts for the plant lipids hydroprocessing. *Nanosystems: Phys. Chem. Math.*, 2025, **16** (6), 872–886.

1. Introduction

Currently, the study of nickel-containing catalysts on zeolites is relevant for the hydroprocessing plant lipids (fatty acids, microalgae lipids, waste cooking oils) to obtain iso-alkanes [1, 2]. This process is carried out to obtain motor fuels similar in their characteristics to diesel and aviation fuels obtained from fossil raw materials [3]. One of the promising supports is the zeolite ZSM-23 [4–6], which, due to its one-dimensional channel system, makes it possible to increase the selectivity of isomerization by suppressing the formation of multibranched alkanes, which can easily be subjected to a side process of hydrocracking. To increase the activity and stability, the catalysts can be modified with transition metals such as Mo [7], W [8], Co [9], Cu [10]. As has been shown in several studies, molybdenum has the greatest effect on the activity of nickel-containing catalysts in the hydroprocessing of plant lipids [7, 11]. Since the nature of metal-support interaction is one of the determining factors in the formation of the dispersed state of the phases of the active component, it is important to know the form the metals in the impregnating solution, as well as charge of the support surface. It is known that surface polarization occurs in an aqueous medium and, depending on the pH of the medium, the support surface can be positively or negatively charged [12]. The pH value at which the surface of the support is not charged is called the point of zero charge (PZC) [13]. In contact with impregnating solutions more acidic than PZC, the surface of the support is positively charged and adsorbs anions. If the impregnating solution is more alkaline than PZC, then the surface of the support is negatively charged and cations are adsorbed [13, 14].

One of the common methods of preparing Ni-Mo catalysts is incipient wetness impregnation, in which the sequence of metal deposition may differ – first Ni, then Mo [15, 16]; first Mo, then Ni [17, 18] and co–precipitation [11, 19–22]. The composition of the impregnation solution may also differ, the most used are aqueous [11, 15–18], citrate [20, 21] and ammonia [19, 22]. All these parameters can affect the distribution of metals on the surface and the degree of their interaction with the support, which in turn will determine the catalytic activity. While the impact of various preparation parameters on traditional hydrodesulfurization (HDS) catalysts has been studied, the influence of these parameters on catalysts designed for the hydroprocessing of plant-based lipids is less well understood. This presents a significant knowledge gap, as the oxygen-rich nature of lipid feedstock and specific reaction pathways, such as deoxygenation, require different demands on catalyst active sites compared to sulfur removal. In particular, the effect of impregnation solution composition on the physicochemical properties and phase evolution of Ni-Mo catalysts optimized for lipid upgrading has not been fully investigated.

The effect of the composition of impregnating solutions on the physico-chemical properties of Ni-Mo catalysts for the hydroprocessing of plant lipids has not been comprehensively discussed in literature. Therefore, the purpose of this work is to study the effect of the composition of impregnating solutions on the formation of phases of the oxide form of active component in Ni-Mo catalysts based on zeolite ZSM-23. This article focuses on the impact of the composition of the impregnation solution on the interaction between the metal and the support, as well as the final distribution of nickel and molybdenum atoms, in order to establish rational design principles for more efficient hydroprocessing catalysts for renewable fuels.

2. Experimental

2.1. Materials

Zeolite ZSM-23 in H^+ form with a SiO_2/Al_2O_3 = 48 was used as a support (Zeolyst International, USA). Nickel (II) nitrate $Ni(NO_3)_2 \cdot 6H_2O$ ($\geq$ 98 %)(Reachim, Russia) and ammonium paramolybdate $(NH_4)_6Mo_7O_{24} \cdot 4H_2O$ ($\geq$ 98 %) (Laverna, Russia) were used as metal precursors. Citric acid $C_6H_8O_7$ (Base No. 1 of Chemical Reagents, Russia) and 25 % ammonia solution (Base No. 1 of Chemical Reagents, Russia) were used as complexing agents. Technical oleic acid (Reachim, Russia) (hereinafter referred to as the FAs mixture) was used as a model raw material, which includes palmitic (5.1 mol. %) (stearic (3.1 mol. %) (oleic (59.2 mol. %) (linoleic (30.4 mol. %) (linolenic acid (1.7 mol. %) (and arachidonic (0.5 mol. %) acids.

2.2. Preparation of catalysts

The catalysts with the following composition – 5 % Ni – 2.5 % Mo/ZSM-23 were prepared by incipient wetness impregnation. One of the samples was prepared by sequentially deposition of metals – first Ni, then Mo. Other samples were prepared by applying an impregnation co-solution in the presence of various complexing agents and with different pH. The NiMo-wat sample was prepared from an aqueous co-solution, the NiMo-cit sample – from a citrate co-solution, NiMo-amm-9 – from an ammonia co-solution with pH = 9, and NiMo-amm-11 – from am ammonia co-solution with pH = 11. After metal deposition, the catalysts were dried at 120 °C for an hour and then calcined at 550 °C for 2 h. Before the catalytic experiments, the samples were reduced *in situ* in a flow of hydrogen (500 ml/min) for an hour at 550 °C at atmospheric pressure. Before physico-chemical studies, the samples were reduced under a hydrogen flow of 500 ml/min for an hour at a temperature of 550 °C at atmospheric pressure, then passivated with ethanol.

2.3. Characterization of the catalysts

The *pH PZC* for zeolite ZSM-23 was determined using the weight titration method [23, 24]. 50 ml of an electrolyte solution (0.01 M NaCl) was added to a 100 ml glass. Then, the zeolite was added to beaker in small portions (0.1 g each) at certain intervals (5 – 10 min) with continuous stirring on a magnetic stirrer, until unchanged pH values of the solution were reached. pH was measured using the Multitest IPL-301 pH meter (Russia). The techniques of temperature-programmed reduction (*TPR*), temperature-programmed desorption of ammonia (*TPD-NH_3*), diffuse reflection spectroscopy in the UV and visible regions (*UV-Vis DRS*), *Raman* and *IR spectroscopy,* X-ray diffraction analysis (*XRD*) were described earlier [25, 26]. The sample microstructure was examined by High-Resolution Transmission Electron Microscopy (HRTEM) using a ThemisZ microscope (Thermo Fisher Scientific, USA) at an accelerating voltage of 200 kV (point-to-point resolution: 0.07 nm).

2.4. Catalytic tests

The catalytic experiments were carried out in a flow reactor. The loading of the catalyst (fraction 0.25 – 0.5 mm) was 1 g. For uniform heat exchange, the catalyst was mixed with quartz (0.63 – 1.0 mm) – 3.8 g. The process was carried out at 300 °C, in a flow of hydrogen and argon (500 and 200 ml/min, respectively). WHSV was 8.4 h^{-1}, the ratio of hydrogen to fatty acids H_2/FAs for standard experiments was 3150 m^3/m^3. The time-on-stream was 10 h. The pressure was 2.5 MPa. The fractional composition of the liquid products of the hydroprocessing was determined by the method of simulated distillation (*Sim-Dist*) [27] The group composition of the liquid products was studied by two-dimensional gas chromatography (*GC×GC*) [27].

3. Results and discussion

3.1. Analysis of impregnating solutions

According to weight titration data, the pH PZC for zeolite ZSM-23 was 4.3. Table 1 shows the pH values of the impregnating solutions. The methods of Raman and IR and UV-vis spectroscopy were used to determine the kind of metal ions in impregnating solutions.

In Fig. 1 and Fig. 2, the IR and Raman spectra of impregnating solutions is shown. In the Raman spectrum of the $Ni(NO_3)_2$ solution, a single band with a maximum of about 1046 cm^{-1} is observed, related to the $n_s(NO_3)$ oscillation of the nitrate ion. In the IR spectrum of this solution, bands of water 1627 cm^{-1} ($\delta(H_2O)$) and nitrate ion 1345 cm^{-1}, 1385 cm^{-1} ($n_s(NO_3)$), 1046 cm^{-1} ($n_s(NO_3)$), 830 cm^{-1} ($\delta_{as}(NO_3)$) are observed [28]. The band of a doubly degenerate

TABLE 1. pH of impregnating solutions

Catalysts	pH of impregnating solutions	
	$Ni(NO_3)_2$	$(NH_4)_6Mo_7O_{24}$
Ni-Mo	5.08	5.24
NiMo-wat	3.92	
NiMo-cit	2.68	
NiMo-amm-9	9.10	
NiMo-amm-11	10.99	

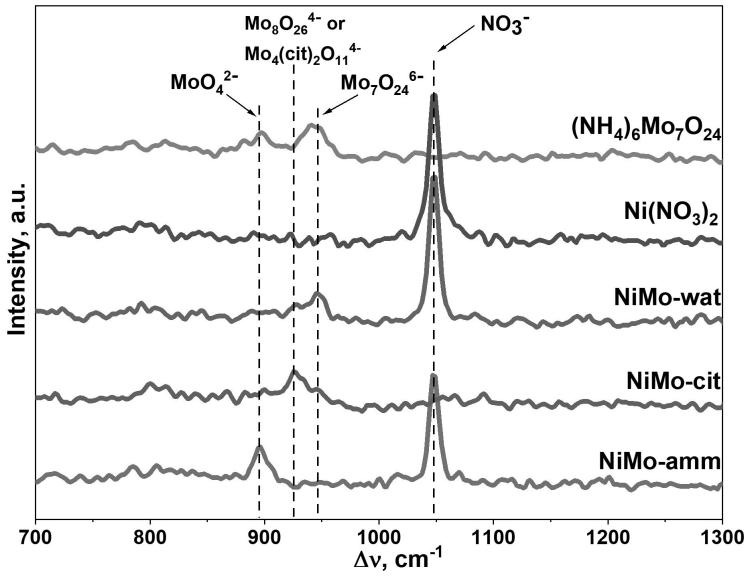

FIG. 1. Raman spectra of impregnating solutions

asymmetric valence oscillation for a free nitrate ion is split into two components (1345 and 1385 cm^{-1}), which indicates the coordination of nitrate ions to nickel cations. Thus, the spectrum corresponds to the compound $Ni(H_2O)_x(NO_3)_y$.

Bands 897 and 944 cm^{-1} are observed in the Raman spectrum of the ammonium paramolybdate solution. Bands 894, 839, 1451 and 1634 cm^{-1} are observed in the IR spectrum of this solution. The appearance of the obtained spectra indicates that both paramolybdate $Mo_7O_{24}{}^{6-}$ (944 cm^{-1} – Raman and 894 cm^{-1} – IR) and monomolybdate $MoO_4{}^{2-}$ (897 cm^{-1} – Raman, 839 cm^{-1} – IR) ions are present in the solution [29]. In addition, ammonium ions (1451 cm^{-1} in IR) and water (1634 cm^{-1} in IR) are present in this solution. A band of paramolybdate 944 cm^{-1} and nitrate 1046 cm^{-1} is observed in the Raman spectrum of NiMo-wat. Bands of paramolybdate 904 and 929 cm^{-1} and nitrate 1382, 1344, 1046 and 830 cm^{-1} and water 1627 cm^{-1} are also observed in the IR spectrum of this solution. The Raman and IR spectra of the NiMo-cit solution correspond to the spectrum of the mixed Ni_xMoCit complex [21]. The spectra of NiMo-amm-9 and NiMo-amm-11 solutions turned out to be similar, therefore, one spectrum is given for an ammonia impregnation solution. The bands $MoO_4{}^{2-}$ 894 cm^{-1} and 1048 cm^{-1} nitrate are observed in the Raman spectrum of the NiMo-amm solution. In the IR spectrum of this solution, in addition to the bands of monomolybdate (827 cm^{-1}) and nitrate (1380, 1346 and 1043 cm^{-1}), a band of NH_3 is observed, probably coordinated to nickel cations (1244 cm^{-1}).

Analyzing the obtained spectra of impregnating solutions and pH PZC for zeolite ZSM-23, a scheme can be proposed for the electrostatic interaction of the surface of zeolite ZSM-23 and metal ions in impregnating solutions (Fig. 3). As mentioned earlier, at pH $<$ PZC, the zeolite surface is positively charged and presumably adsorbs anions on its surface. At pH $>$ PZC, the zeolite surface is negatively charged and preferentially adsorbs cations. According to the IR and Raman spectra, in solutions with a pH below 7, molybdenum mainly presents in the form of polymolybdate anions $[Mo_7O_{24}]^{6-}$ and $[Mo_8O_{26}]^{4-}$. In solutions with a pH greater than 7, molybdenum presents mainly in the form of monomolybdate ion $[MoO_4]^{2-}$. Thus, 3 groups of catalysts can be distinguished in accordance with the charge of the zeolite surface and the state of molybdenum in the impregnation solution during preparation. The first group of catalysts includes samples in which, during preparation, the zeolite surface is positively charged, and molybdenum is in the form of polymolybdate ions. These are NiMo-wat and NiMo-cit catalysts. The second group includes catalysts, in which the zeolite surface is

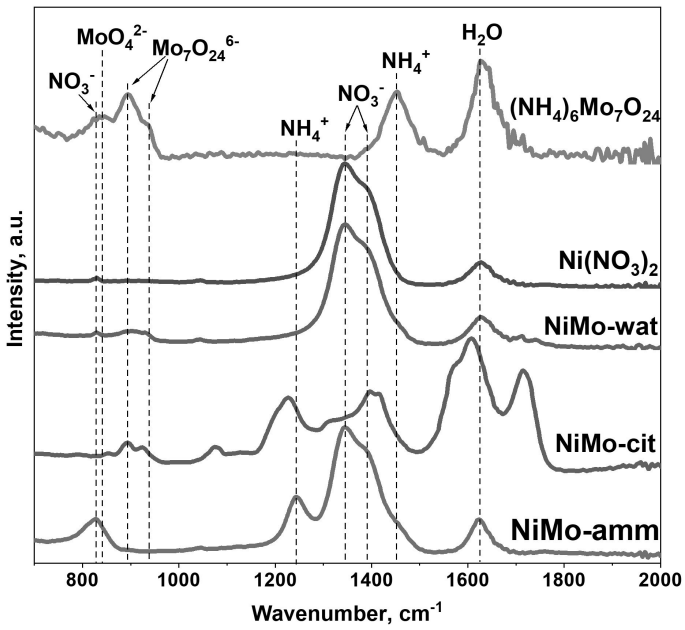

FIG. 2. IR spectra of impregnating solutions

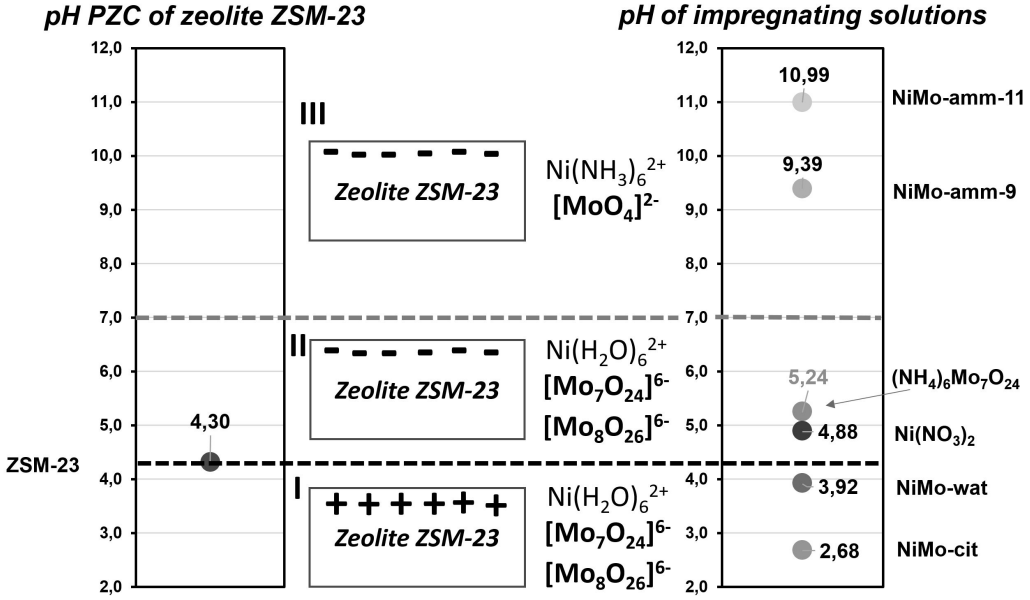

FIG. 3. Scheme of electrostatic interaction of zeolite ZSM-23 and metal ions in impregnating solutions

negatively charged during preparation, and molybdenum is in the form of polymolybdate ions. This is a sample of Ni-Mo. The third group includes catalysts, in which the zeolite surface is negatively charged during preparation, and molybdenum is in the form of monomolybdate ions. These are the NiMo-amm-9 and NiMo-amm-11 samples. It can be expected that the most uniform distribution of nickel and molybdenum will be in the 3rd group of catalysts, since the charge value of metal ions is the same ($[Ni(NH_3)_6]^{2+}$ and $[MoO_4]^{2-}$), which can lead to the formation of a complex with a metal ratio Ni/Mo = 1. In the case of other catalysts, the charge value of the paramolybdate ion is higher ($[Mo_7O_{24}]^{6-}$, $[Mo_8O_{26}]^{4-}$ and $[Ni(H_2O)_6]^{2+}$), therefore, most likely, complexes with a metal ratio of Ni/Mo = 3 will form in the solution.

3.2. UV-vis spectroscopy

To obtain information on the coordination of metal atoms, UV-vis spectra for Ni-Mo/ZSM-23 catalysts in oxide form were recorded. For all catalysts, two main absorption regions can be distinguished – from 10000 to 30000 cm^{-1} (Fig. 4a) and from 30000 to 45000 cm^{-1} (Fig. 4b). In the first absorption region (visible range), due to the manifestation of d-d transitions of Ni^{2+} cations, several main absorption bands can be distinguished. The band at 13800 cm^{-1} corresponds

to Ni^{2+} particles stabilized in an octahedral oxygen environment ($Ni^{2+}O_h$), and the band at 15200 cm^{-1} corresponds to Ni^{2+} particles in a tetrahedral oxygen environment ($Ni^{2+}T_d$). Also, in the spectra of all bimetallic catalysts, there is a wide absorption band at 12220 cm^{-1}, which corresponds to distorted octahedral $Ni^{2+}(O_h)$ particles, which is associated with the formation of a joint Ni-Mo phase in the form of $NiMoO_4$ [30,31]. The intensity of the absorption band may indirectly indicate the size and availability of metal particles. Thus, the lowest absorption in the region of 10000 – 15000 cm^{-1} is observed for the Ni-Mo catalyst, which may indicate the blocking of nickel particles by molybdenum particles [32]. The highest absorption in this region is observed for NiMo-amm-9, which may indicate the most dispersed nickel particles.

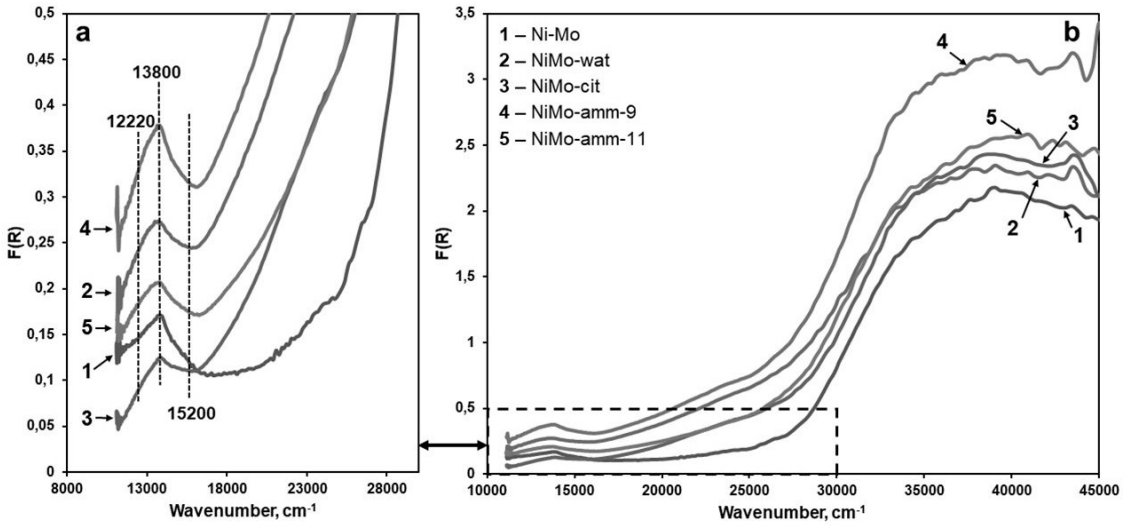

FIG. 4. UV-vis spectra of NiMo/ZSM-23 catalysts in oxide form in the range: (a) from 10000 to 30000 cm^{-1}, (b) from 10000 to 45000 cm^{-1}

The second absorption region (UV range) is usually due to the manifestation of charge transfer bands of ligand-metal cations Ni^{2+} or Mo^{6+} or the general absorption of massive systems such as NiO oxide or MoO_3 [7, 32, 33]. The most intense absorption in this area is observed for the NiMo-amm-9 catalyst. This may be due to the formation of monomolybdates $[MoO_4]^{2-}$ in an ammonia impregnation solution, which, when calcined, form smaller particles compared to particles obtained from polymolybdates $[Mo_7O_{24}]^{6-}$ and $[Mo_8O_{24}]^{4-}$ [31]. It is difficult to identify absorption bands for octahedral and tetrahedral forms of molybdenum Mo^{6+} cations, since these bands are poorly expressed due to the small amount of molybdenum in catalysts.

3.3. Raman spectroscopy

The catalysts in the oxide form were investigated by Raman spectroscopy to determine the types of metal particles in the samples. In the spectra (Fig. 5) of all catalysts, a band at 961 cm^{-1} is observed, which refers to V_s (Mo=O) oscillations of the α-$NiMoO_4$ phase [11, 34, 35]. A small band at 914 cm^{-1} is also found in the spectra of the NiMo-amm-9 and NiMo-amm-11 catalysts, which corresponds to V_a(Mo=O) oscillations of the α-$NiMoO_4$ phase [11, 34]. The appearance of additional bands indicates an increase in the amount of α-$NiMoO_4$ phase in the NiMo-amm-9 and NiMo-amm-11 catalysts. Trace amounts of the β-$NiMoO_4$ phase may also be present in all samples, fluctuations of which should be observed at 900 and 945 cm^{-1} [35,36]. It is worth noting that with an increase in the pH of the ammonia impregnation solution, the intensity of the α-$NiMoO_4$ phase band increases, which may indicate an increase in its amount. No oscillation bands related to the MoO_3 phase were detected.

3.4. Temperature-programmed reduction

For all catalysts on the TPR profiles (Fig. 6), hydrogen absorption in the range from 150 to 350 °C is not observed, which indicates the absence of massive NiO particles [18]. The rest of the TPR profile can be divided into 4 components.

The particles of of nickel oxides weakly bound to the surface of the support [17, 22, 37] are reduced at temperatures of 350 – 450 °C. In the case of NiMo-cit catalyst, the absence of this reduction maximum may be due to the formation of a Ni_xMoCit complex in the impregnation solution, by analogy with $Co_2[Mo_4O_{11}(C_6H_5O_7)_2]$ [38], from which, upon calcination, co-oxides of Ni and Mo or particles of $NiMoO_4$ are formed [7,39]. The next maximum reduction in the region of 450 – 520 °C corresponds to the reduction of interacting NiO and MoO_3 particles. Interaction can be understood as both physical contact between particles [25] and chemical interaction – the formation of the $NiMoO_4$ phase [40]. Further, at a temperature of about 560 °C, Mo^{6+} is reduced to Mo^{4+} [17, 37, 41], which corresponds to the reduction of molybdenum oxide particles that do not encounter nickel-containing particles. At temperatures of 700 – 750 °C, molybdenum is further reduced to a metallic state [7, 18, 41]. It is also worth noting that the amount of hydrogen absorbed differs from catalyst

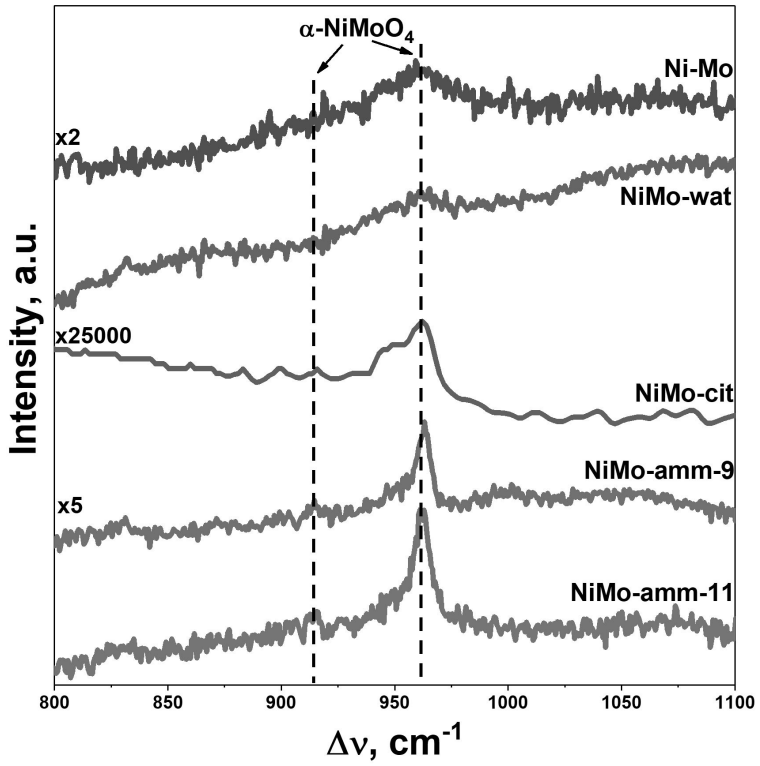

FIG. 5. Raman spectra of NiMo/ZSM-23 catalysts in oxide form

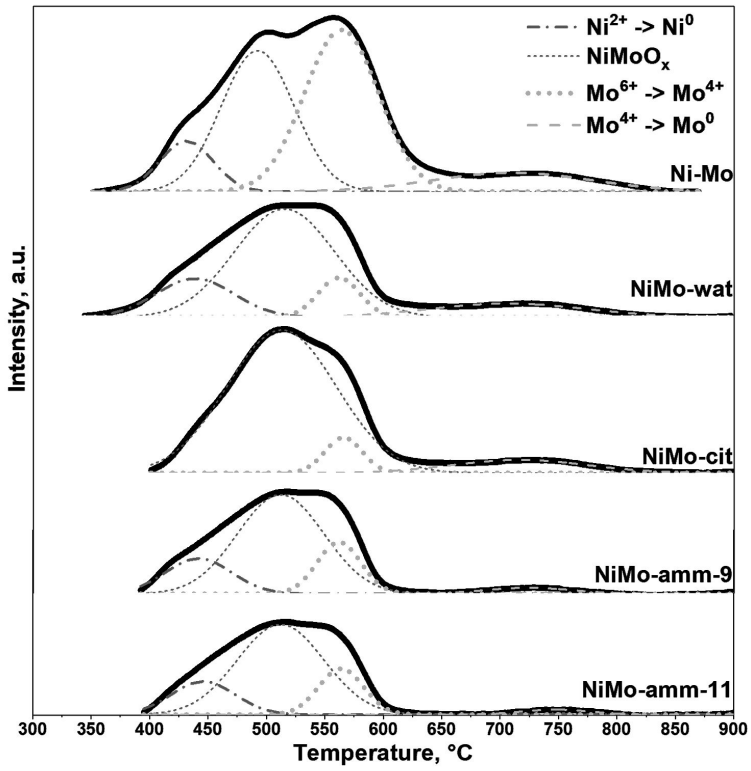

FIG. 6. Decomposed TPR profiles of NiMo/ZSM-23 catalysts in oxide form

to catalyst. The largest amount of absorbed hydrogen is observed for the Ni-Mo sample. In the case of impregnation co-solutions, the smallest amount of absorbed hydrogen is observed for samples NiMo-amm-9 and NiMo-amm-11. This may indicate that in catalysts prepared from ammonia impregnation solutions, there is a stronger interaction of the active component with the surface of the support compared to other samples [42].

3.5. X-ray diffraction analysis

All diffractograms (Fig. 7) show the reflexes of the support – ZSM-23. For all catalysts, a peak at 37.2° can be identified, which refers to 111 NiO (PDF 47-1049). However, for the catalysts prepared by impregnation co-solutions, this peak is weakly expressed. This may indicate the presence of highly dispersed NiO particles, or a smaller number of them than in the Ni-Mo catalyst. Also, for all catalysts, a peak is observed at 26.7°, which corresponds to β-$NiMoO_4$ (PDF 45-142). For the NiMo-amm-9 and NiMo-amm-11 catalysts, a peak at 28.8° can be distinguished, which belongs to α-$NiMoO_4$ (PDF 9-175). Since the diffractograms show relatively weak signals from phases containing nickel and molybdenum, which also overlap with peaks of the support, the intensity ratio of certain phase peaks was used for only qualitative comparison of catalysts. The evaluation method is described in detail in the experimental part. As a comparison, Table 2 shows the ratio of intensities (I) at various points for the zeolite, the remaining samples were analyzed relative to this "control point".

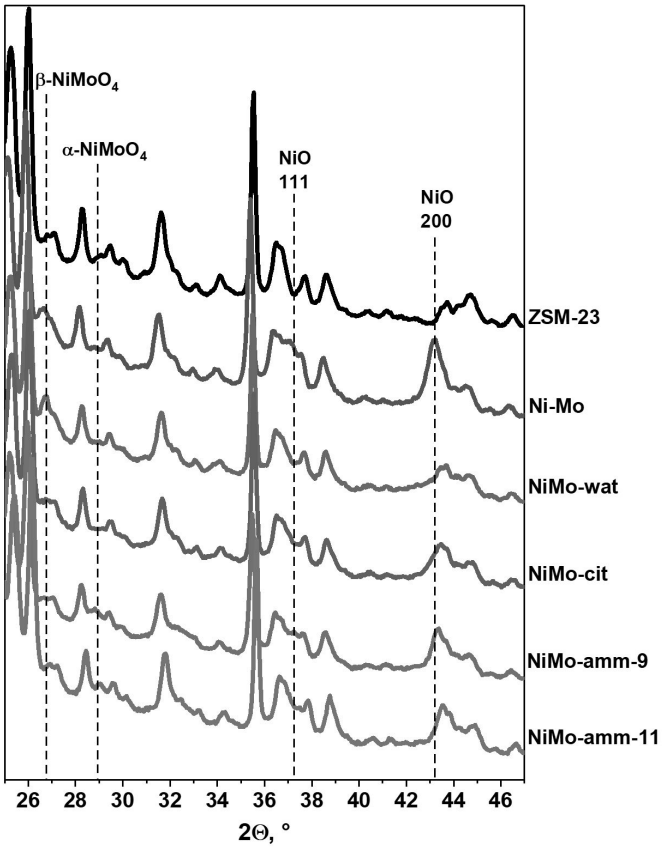

FIG. 7. Diffractograms of NiMo/ZSM-23 catalysts in oxide form

Based on the data given in Table 2, the β-$NiMoO_4$ phase can be identified in all catalysts. The α-$NiMoO_4$ phase presents only in catalysts prepared from ammonia impregnation co-solutions. It is known that pure β-$NiMoO_4$ is a metastable phase that exists at high temperature [43]. However, with an excess of nickel in the catalyst (atomic ratio Mo/(Ni+Mo) < 0.5), the β-$NiMoO_4$ phase can be stable at room temperature [44, 45]. Apparently, nickel-enriched particles forming the β-$NiMoO_4$ phase are present in all catalysts. In the catalysts NiMo-amm-9 and NiMo-amm-11, nickel and molybdenum are distributed more evenly, which allows obtaining the stoichiometric phase α-$NiMoO_4$. The observed phenomenon regarding the formation of phases is consistent with the previously proposed scheme of electrostatic interaction of metals in solution and with the surface of the support.

Figure 8 shows X-ray images of Ni-Mo/ZSM-23 catalysts in reduced form. Narrow peaks of the support (zeolite ZSM-23) are present on all diffractograms. For all catalysts, a peak is observed at 44.1°, which corresponds to (111) Ni (PDF 04-0850). A peak at 51.7° is also observed for the Ni-Mo sample, corresponding to (200) Ni (PDF 04-0850). Reflexes corresponding to the molybdenum-containing phases are not observed.

TABLE 2. Structural characteristics of NiMo/ZSM-23 catalysts in oxide form

Catalyst	I(β-$NiMoO_4$)/ I(ZSM-23)	I(α-$NiMoO_4$)/ I(ZSM-23)	I(NiO)/ I(ZSM-23)	I(β-$NiMoO_4$)/ I(α-$NiMoO_4$)	Phase composition	CSD, Å
ZSM-23	0.48	0.03	0.32	—	ZSM-23	—
5Ni-ZSM-23	0.39	−0.05	1.98	—	NiO ZSM-23	300
Ni-Mo	0.95	−0.05	1.55	—	NiO β-$NiMoO_4$ ZSM-23	160
NiMo-wat	1.32	−0.06	0.62	—	NiO β-$NiMoO_4$ ZSM-23	60
NiMo-cit	0.76	−0.01	0.82	—	NiO β-$NiMoO_4$ ZSM-23	90
NiMo-amm-9	0.64	0.25	0.99	2.6	NiO α-$NiMoO_4$ β-$NiMoO_4$ ZSM-23	170
NiMo-amm-11	0.69	0.21	0.65	3.3	NiO α-$NiMoO_4$ β-$NiMoO_4$ ZSM-23	110

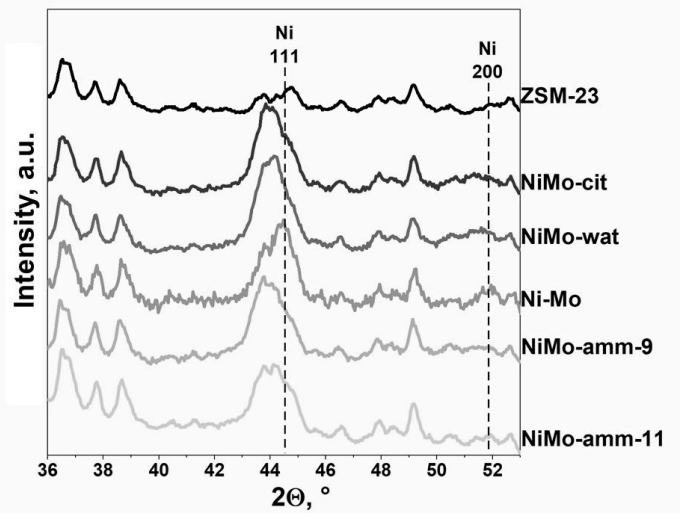

FIG. 8. Diffractograms of NiMo/ZSM-23 catalysts in reduced form

The structural characteristics of the reduced catalysts are presented in Table 3. The lattice parameter for pure nickel is 3.523 Å. For the Ni-Mo sample, this parameter is practically the same, which may indicate the absence of Ni-Mo solid co-solutions. For the remaining samples, the lattice parameter is greater than that of pure nickel, which is associated with the formation of solid co-solutions.

Apparently, this is because nickel and molybdenum, being in the same impregnation solution, can interact to form various complexes, which, when fixed on the surface and further calcination, give solid solutions. It can also be noted that the use of impregnation co-solutions helps to reduce the size of CSD for nickel particles.

3.6. High-resolution transmission electron microscopy

To determine the distribution of metals on the surface of zeolite ZSM-23, catalysts in oxide form were studied by HRTEM. The resulting images and the energy dispersive X-ray (EDX) mapping analysis data of the studied samples are shown in the Fig. 9. The average size of Ni- and Mo-containing particles is represented in Table 4.

The largest size (Table 4) – 14 nm – of metal-containing particles is observed in the Ni-Mo catalyst, which is prepared by successive deposition of Ni and Mo. Smaller particles are observed in the other catalysts prepared from impregnation

TABLE 3. Structural characteristics of NiMo/ZSM-23 catalysts in reduced form

Sample	Phase composition	Lattice parameter, Å	CSD, Å	x in $Ni_{1-x}Mo_x$
Ni-Mo	ZSM-23 Ni	3.528	120	0.01
NiMo-wat	ZSM-23 Ni	3.562	80	0.08
NiMo-cit	ZSM-23 Ni	3.567	100	0.09
NiMo-amm-9	ZSM-23 Ni	3.575	70	0.11
NiMo-amm-11	ZSM-23 Ni	3.571	70	0.10

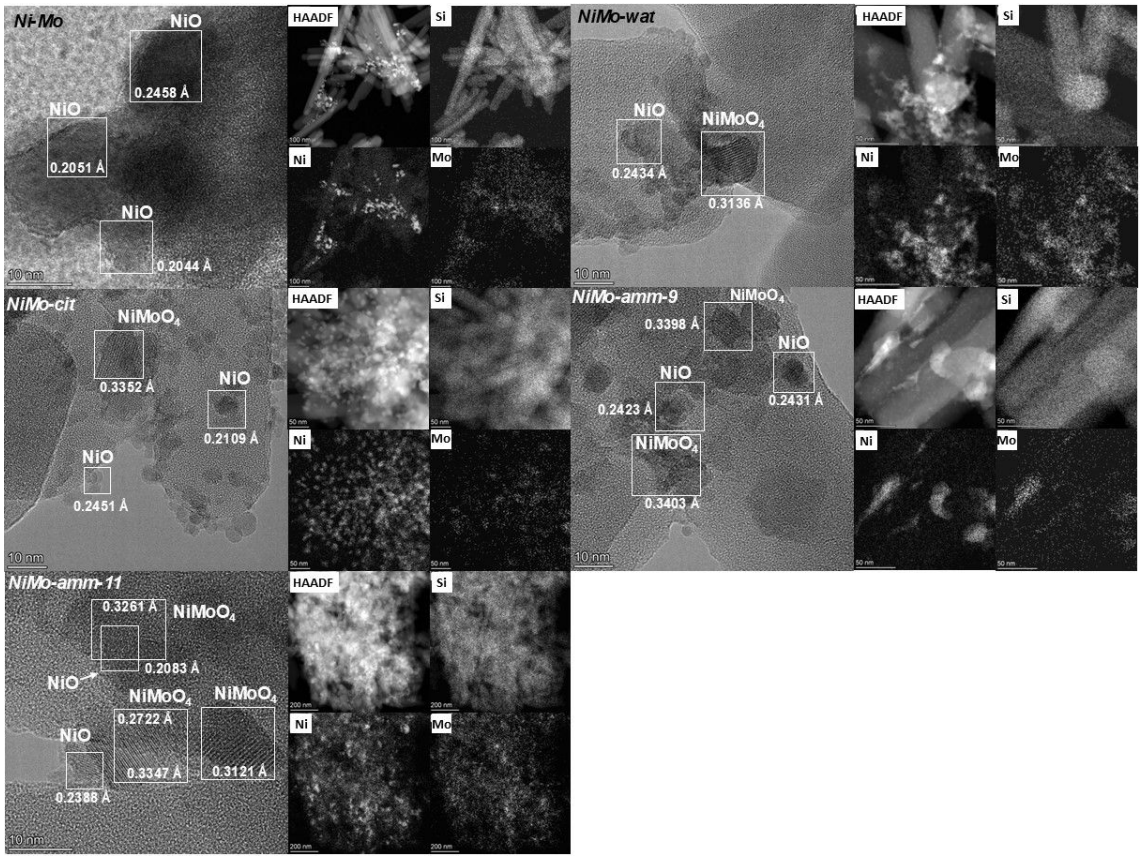

FIG. 9. HRTEM and EDX images for NiMo/ZSM-23 catalysts in oxide form

TABLE 4. Average particle size (HRTEM) for NiMo/ZSM-23 catalysts in oxide form

Catalyst	Average particle size, nm
Ni-Mo	14.1 ± 0.2
NiMo-wat	3.4 ± 0.1
NiMo-cit	3.5 ± 0.1
NiMo-amm-9	3.2 ± 0.1
NiMo-amm-11	3.1 ± 0.1

co-solutions. The determination of the interplane distance showed that in the Ni-Mo catalyst, most of the particles are a phase of nickel oxide. Molybdenum, in the form of a phase of molybdenum oxides, has a dispersed distribution and is localized on the surface of NiO particles and the surface of the support. $NiMoO_4$ particles are also observed for NiMo-wat and NiMo-cit catalysts. For catalysts prepared from ammonia impregnation solutions, $NiMoO_4$ particles are mainly observed in HRTEM images, and to a lesser extent, NiO particles. Thus, the use of impregnation co-solutions contributes to the formation of joint Ni-Mo phases. The use of ammonia impregnating solutions leads to a more uniform particle size distribution and the formation of mainly joint Ni-Mo phases.

According to the EDX mapping data, the distribution of Ni and Mo is quite close for the NiMo-cit and NiMo-wat samples – Ni- and Mo-containing particles with close boundaries and positions could be observed. The main differences were observed for the Ni-Mo sample. On the one hand, Ni-containing particles were found. On the other hand, the distribution of Mo-containing particles was very uniform and close to the distribution of Si, which may mean that Mo is uniformly distributed on the surface of the oxides in contrast to Ni. The distribution of Ni and Mo was close in the case of NiMo-amm-11 and quite uniform for both elements, which is in good agreement with our assumption of more uniform distribution of Ni and Mo in the case of using ammonia impregnating solution.

3.7. Temperature-programmed desorption of ammonia

The number of acid centers (AC) in the reduced catalysts was determined using temperature-programmed desorption of ammonia. The obtained TPD-NH_3 profiles are shown in Fig. 10.

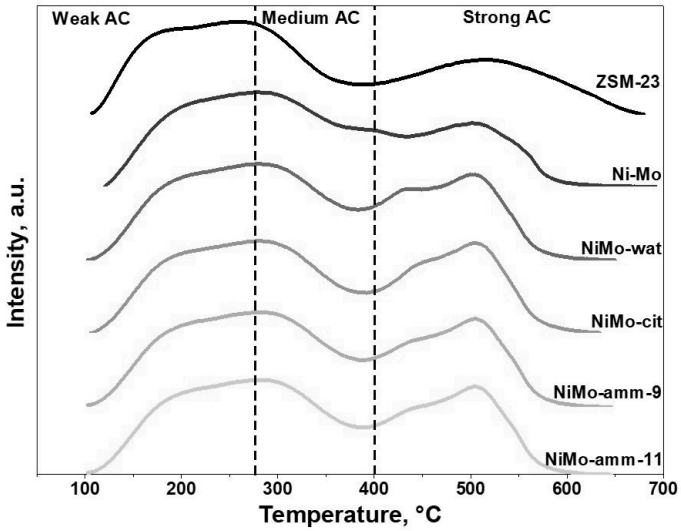

FIG. 10. TPD-NH_3 profiles of zeolite ZSM-23 and reduced catalysts

Table 5 shows the amount of desorbed ammonia from various zeolite centers and reduced catalysts. The acid centers of zeolite can be divided into 3 groups according to strength: weak, from which ammonia is desorbed at temperatures below 275 °C, medium (275 – 400 °C) and strong (over 400 °C) [4, 5, 46–48]. TPD-NH_3 profiles exhibit two clearly distinguishable desorption maxima, which correspond to typical TPD profiles for this zeolite [46–48]. The first maximum is in the temperature range of 100 – 350 °C and corresponds to the desorption of ammonia from weak and medium AC. The high-temperature peak of ammonia desorption, observed in the range of 350 – 550 °C, corresponds to medium and strong AC [46–48].

For all catalysts, compared with zeolite ZSM-23, there is a decrease in the number of weak and strong AC. This takes place because metal particles interact with these types of AC during application, thereby blocking them [49]. An increase in the number of average AC is observed for all samples. Also, transition metal-based catalysts usually have increased low and medium acidity due to the appearance of weak acid centers of transition metals [50, 51]. The increase in the number of average AC may also be due to the presence of MoO_x particles in the catalyst [52, 53].

3.8. Catalytic tests

The component composition of the liquid organic product obtained at the 10^{th} (last) hour of the process is shown in Table 6. The following groups of compounds were found in the organic phase: alkanes, isoalkanes, alkenes, cycloalkanes, aromatic compounds and O-containing compounds – fatty acids, esters of fatty acids, lactones, alcohols. C_6-C_{15} fatty acids are formed as a result of hydrocracking of the initial C_{16}-C_{18} fatty acids. Alcohols are formed as a result of hydrogenation of fatty acids and are an intermediate product of deoxygenation [17]. Esters can be formed from fatty acids (initial and shorter ones) and alcohols, which are obtained in the hydroprocessing from fatty acids [17]. Lactones

TABLE 5. The number of acid centers according to TPD-NH_3

Sample	Desorbed amount of NH_3, mmol/g			
	Weak AC	Medium AC	Strong AC	Σ
ZSM-23	503	164	288	955
Ni-Mo	454	207	183	744
NiMo-wat	488	201	220	910
NiMo-cit	465	182	217	864
NiMo-amm-9	475	191	215	881
NiMo-amm-11	482	196	217	895

are internal cyclic esters and can be formed from fatty acids [54]. C_{15}-C_{18} linear alkanes are formed from the initial C_{16}-C_{18} fatty acids through the deoxygenation stage. C_5-C_{14} linear alkanes are formed as a result of hydrocracking of linear alkanes C_{15}-C_{18}, as well as from fatty acids with a shorter chain length than in the initial mixture. Alkenes are intermediates of hydrocracking and hydroisomerization processes [55]. C_5-C_{18} isoalkanes are formed during the hydroisomerization of the corresponding linear alkanes. Aromatic compounds are products of alkene dehydrocyclization. Cycloalkanes can be products of hydrogenation of aromatic compounds [1, 56].

The content of O-containing compounds in a liquid organic product differs for catalysts prepared by different methods. The lowest content of O-containing compounds is observed when using a Ni-Mo catalyst (9.4 wt. %). In the case of using NiMo-amm-9 and NiMo-amm-11 catalysts, a slight increase in the amount of O-containing compounds is observed – 12.4 and 13.7 wt. %, respectively. The least active catalysts are NiMo-wat and NiMo-cit, for which the amount of O-containing compounds is 32.6 and 49.3 wt. %, respectively. This behavior of catalysts may be related to the varying degrees of interaction of molybdenum particles with the surface of the support. According to the scheme of electrostatic interaction (Fig. 3), during the preparation of NiMo-wat and NiMo-cit catalysts, molybdenum in the form of polymolybdate ions ($[Mo_7O_{24}]^{6-}$ and $[Mo_8O_{26}]^{4-}$) interacts with the positively charged surface of ZSM-23 zeolite, which can lead to a strong metal-support interaction [57, 58]. As a result, the ability to activate O-containing compounds may decrease. It was previously shown that the active phase of the oxide precursors of sulfide hydrotreating catalysts can directly affect the activity of the final catalysts in the hydrotreating process. It was shown that massive sulfided Ni-Mo catalyst is active in the hydroprocessing of sulfide model compounds in the series of works [59, 60]. At the same time, the composition of the sample contained both α-$NiMoO_4$ and β-$NiMoO_4$ phases in the oxide form, but the β-$NiMoO_4$ phase was the main one. Apparently, in our case, the interaction of the molybdate phases with the support can stabilize the α-$NiMoO_4$ phase in some cases (Table 2), which also leads to a change in the selectivity towards oxygen-containing compounds (Table 6).

The target products of the hydroprocessing are isoalkanes. The smallest amount of iso-alkanes is observed when using NiMo-wat and NiMo-cit catalysts. Apparently, this is due to their low activity, which is confirmed by the amount of O-containing compounds in the liquid organic product. The largest amount of isoalkanes is observed in the case of using the NiMo-amm-11 catalyst (35.2 wt. %)(which may be due to its higher acidity than that of the Ni-Mo and NiMo-amm-9 samples (Table 5). On the one hand, previous studies have demonstrated the influence of zeolite-type catalyst support acidity on the yield of isomerized alkanes produced from vegetable oils [61]. On the other hand, it has also been shown that metal incorporation into catalyst supports, such as tungsten, can directly affect their acidity, and consequently, the yield of isomerized alkanes during the hydroprocessing of sunflower oil with using Pt/WO_x-Al_2O_3 catalysts [62].

Thus, from the point of view of the composition of the liquid organic phase, the NiMo-amm-11 catalyst is the most promising. Despite the fact that the amount of O-containing compounds on this catalyst was not minimal (13.7 wt. %) (the content of isoalkanes in the liquid organic product turned out to be maximum (35.2 wt. %).

Figure 11 shows the change in the fractional composition of the liquid organic product obtained at the 10^{th} (last) hour of the process, depending on the catalyst. The largest proportion of the "diesel" fraction is observed in liquid organic products produced on Ni-Mo, NiMo-amm-9 and NiMo-amm-11 catalysts. Liquid organic products produced on NiMo-wat and NiMo-cit catalysts have a high content of "vacuum gasoil" and "vacuum residue". This behavior of the fractional composition is consistent with the data of two-dimensional gas chromatography, where a similar dependence of the amount of O-containing compounds on the catalyst was observed.

TABLE 6. Composition of the liquid organic phase at the 10^{th} (last) hour of the process, according to two-dimensional gas chromatography data

Sample	Ni-Mo	NiMo-wat	NiMo-cit	NiMo-amm-9	NiMo-amm-11
Compound	wt. %				
O-containing compounds:	**9.4**	**32.6**	**49.3**	**12.4**	**13.7**
C_6-C_{15} FAs	0.0	0.0	0.0	0.0	0.3
C_8-C_{35} lactones	2.7	7.6	9.8	3.5	3.3
C_{20}-C_{45} esters of FAs	4.9	20.9	34.1	6.5	5.6
C_9-C_{35} alcohols	0.6	1.1	2.3	0.7	0.2
C_{16}-C_{20} initial FAs	1.2	3.0	3.1	1.7	4.3
Hydrocarbons total:	**90.6**	**67.4**	**50.7**	**87.6**	**86.3**
C_{10}-C_{25} cycloalkanes	3.5	3.8	1.7	3.0	1.1
C_6-C_{20} aromatics	3.4	1.2	1.7	2.4	0.0
C_5-C_{18} alkanes	35.0	19.7	17.0	28.6	26.9
C_5-C_{18} isoalkanes	30.4	17.8	12.2	27.1	35.2
C_5-C_{18} alkenes	18.3	24.9	18.1	26.5	23.1
i/n C_5-C_{18}	**0.9**	**0.9**	**0.7**	**0.9**	**1.3**
C_5-C_8 alkanes	0.6	0.5	0.4	0.6	0.7
C_5-C_8 isoalkanes	0.2	0.1	0.1	0.1	0.2
C_5-C_8 alkenes	0.2	0.2	0.1	0.2	0.8
i/n C_5-C_8	**0.3**	**0.2**	**0.1**	**0.2**	**0.3**
C_9-C_{14} alkanes	1.1	0.6	0.5	1.0	0.9
C_9-C_{14} isoalkanes	0.9	0.4	0.3	0.6	0.6
C_9-C_{14} alkenes	2.1	1.8	1.1	2.3	3.0
i/n C_9-C_{14}	**0.8**	**0.6**	**0.5**	**0.6**	**0.6**
C_{15}-C_{18} alkanes	33.3	18.6	16.1	27.1	25.3
C_{15}-C_{18} isoalkanes	29.3	17.4	11.9	26.4	34.4
C_{15}-C_{18} alkenes	16.0	22.9	16.9	24.0	19.4
i/n C_{15}-C_{18}	**0.9**	**0.9**	**0.7**	**1.0**	**1.4**
Yield of liquid organic product	**83.3**	**87.7**	**90.1**	**85.8**	**85.4**

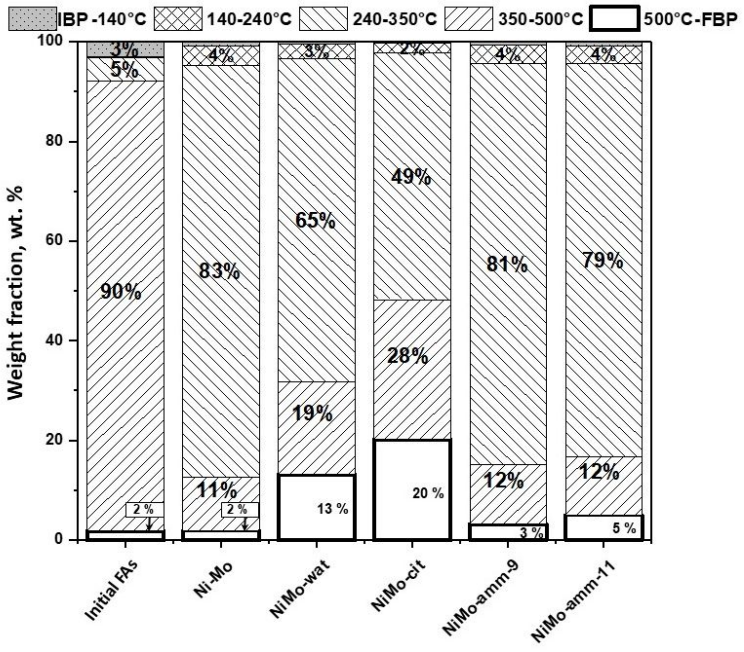

FIG. 11. Fractional composition of the liquid organic phase obtained at the 10^{th} (last) hour of the process, according to SimDist

4. Conclusion

In this work, a series of Ni-Mo catalysts based on zeolite ZSM-23 was synthesized by incipient wetness impregnation using various impregnation solutions. Aqueous, citrate, and ammonia solutions with different pH were used as impregnation solutions. According to IR and Raman spectroscopy data, in impregnating solutions with a pH of less than 7 (aqueous and citrate solutions), nickel is represented as the $Ni(H_2O)_6{}^{2+}$ ion, and molybdenum is present as polymolybdate ions ($[Mo_7O_{24}]^{6-}$ and $[Mo_8O_{26}]^{4-}$). In solutions with a pH of more than 7 (ammonia solutions), nickel is present as the $Ni(NH_3)_6{}^{2+}$ ion, and molybdenum is present as the monomolybdate ion ($[MoO_4]^{2-}$).

Using the XRD and HRTEM methods, the effect of the composition of the impregnation solution on the formation of phases of the metal component was shown. According to the HRTEM data, NiO particles are mainly observed in the catalyst prepared by the method of sequential deposition of metals. According to the XRD data, in addition to the NiO phase, the β-$NiMoO_4$ phase is also observed. The use of aqueous and citrate impregnation solutions leads to the formation of nickel oxide and β-$NiMoO_4$ phases (XRD data). When using ammonia impregnation solutions, the formation of NiO, α-$NiMoO_4$ and β-$NiMoO_4$ phases is observed (XRD data). In addition, according to the HRTEM, the use of ammonia impregnation solutions leads to a decrease in the size of metal-containing particles, as well as to a more uniform distribution of nickel and molybdenum over the surface of the support.

During the hydroprocessing of a mixture of fatty acids (C_{16}-C_{18}) in a flow-type reactor (300 °C, 2.5 MPa, WHSV = 8.4 h^{-1}), the greatest conversion and, consequently, the least amount of O-containing compounds were observed on the Ni-Mo catalyst. The highest yield of the "diesel" fraction was observed using Ni-Mo, NiMo-amm-9 and NiMo-amm-11 catalysts. The highest yield of isoalkanes was observed when using the NiMo-amm-11 catalyst. Thus, from the point of view of fractional and component compositions, as well as the material balance, the NiMo-amm-11 catalyst is the most promising.

References

[1] Yeletsky P.M., Kukushkin R.G., Yakovlev V.A., Chen B.H. Recent Advances in One-Stage Conversion of Lipid-Based Biomass-Derived Oils into Fuel Components — Aromatics and Isomerized Alkanes. *Fuel*, 2020, **278** (1), 118255.

[2] Kordulis C., Bourikas K., Gousi M., Kordouli E., Lycourghiotis A. Development of Nickel Based Catalysts for the Transformation of Natural Triglycerides and Related Compounds into Green Diesel: A Critical Review. *Appl. Catal. B*, 2016, **181**, P. 156–196.

[3] Zhou Y., Remón J., Jiang Z., Matharu A.S., Hu C. Tuning the Selectivity of Natural Oils and Fatty Acids/Esters Deoxygenation to Biofuels and Fatty Alcohols: A Review. *Green Energy and Environment*, 2023, **8** (3), P. 722–743.

[4] Zhang M., Chen Y., Wang L., Zhang Q., Tsang C.W., Liang C. Shape Selectivity in Hydroisomerization of Hexadecane over Pt Supported on 10-Ring Zeolites: ZSM-22, ZSM-23, ZSM-35, and ZSM-48. *Ind. Eng. Chem. Res.*, 2016, **55** (21), P. 6069–6078.

[5] Gao S.B., Zhao Z., Lu X.F., Chi K.B., Duan A.J., Liu Y.F., Meng X.B., Tan M.W., Yu H.Y., Shen Y.G., Li M.C. Hydrocracking Diversity in N-Dodecane Isomerization on Pt/ZSM-22 and Pt/ZSM-23 Catalysts and Their Catalytic Performance for Hydrodewaxing of Lube Base Oil. *Pet. Sci.*, 2020, **17** (6), P. 1752–1763.

[6] Romero D., Rohling R., Meng L., Rigutto M., Hensen E.J.M. Shape Selectivity in Linear Paraffins Hydroconversion in 10-Membered-Ring Pore Zeolites. *J. Catal.*, 2021, **394**, P. 284–298.

[7] Raikwar D., Munagala M., Majumdar S., Shee D. Hydrodeoxygenation of Guaiacol over Mo, W and Ta Modified Supported Nickel Catalysts. *Catal. Today*, 2019, **325**, P. 117–130.

[8] Yang Y., Wang Q., Zhang X., Wang L., Li G. Hydrotreating of C_{18} Fatty Acids to Hydrocarbons on Sulphided NiW/SiO_2-Al_2O_3. *Fuel Processing Technology*, 2013, **116**, P. 165–174.

[9] Zhang Z., Bi G., Zhang H., Zhang A., Li X., Xie J. Highly Active and Selective Hydrodeoxygenation of Oleic Acid to Second Generation Bio-Diesel over SiO_2-Supported $Co_xNi_{1-x}P$ Catalysts. *Fuel*, 2019, **247**, P. 26–35.

[10] Zheng Y., Wang J., Liu C., Lu Y., Lin X., Li W., Zheng Z. Efficient and Stable Ni-Cu Catalysts for Ex Situ Catalytic Pyrolysis Vapor Upgrading of Oleic Acid into Hydrocarbon: Effect of Catalyst Support, Process Parameters and Ni-to-Cu Mixed Ratio. *Renew Energy*, 2020, **154**, P. 797–812.

[11] Cao X., Long F., Zhai Q., Liu P., Xu J., Jiang J. Enhancement of Fatty Acids Hydrodeoxygenation Selectivity to Diesel-Range Alkanes over the Supported Ni-MoO_x Catalyst and Elucidation of the Active Phase. *Renew Energy*, 2020, **162**, P. 2113–2125.

[12] Brunelle J.P. Preparation of Catalysts by Metallic Complex Adsorption on Mineral Oxides. *Pure & Appl. Chem.*, 1978, **50**, P. 1211–1229.

[13] Kyriakopoulos J., Panagiotou G., Petsi T., Bourikas K., Kordulis C., Lycourghiotis A. The Influence of Impregnation Temperature on the PZC of Titania and the Loading of Ni upon Preparation of Ni/TiO_2 Catalysts. *Stud. Surf. Sci. Catal.*, 2010, **175**, P. 643–646.

[14] Hao X., Quach L., Korah J., Spieker W.A., Regalbuto J.R. The Control of Platinum Impregnation by PZC Alteration of Oxides and Carbon. *J. Mol. Catal. A Chem.*, 2004, **219** (1), P. 97–107.

[15] Li K., Wang R., Chen J. Hydrodeoxygenation of Anisole over Silica-Supported Ni_2P, MoP, and NiMoP Catalysts. *Energy and Fuels*, 2011, **25** (3), P. 854–863.

[16] Wang X., Zhao Z., Chen Z., Li J., Duan A., Xu C., Gao D., Cao Z., Zheng P., Fan J. Effect of Synthesis Temperature on Structure-Activity-Relationship over NiMo/γ-Al_2O_3 Catalysts for the Hydrodesulfurization of DBT and 4.6-DMDBT. *Fuel Processing Technology*, 2017, **161**, P. 52–61.

[17] Kordouli E., Sygellou L., Kordulis C., Bourikas K., Lycourghiotis A. Probing the Synergistic Ratio of the NiMo/γ-Al_2O_3 Reduced Catalysts for the Transformation of Natural Triglycerides into Green Diesel. *Appl. Catal. B*, 2017, **209**, P. 12–22.

[18] Qu L., Zhang W., Kooyman P.J., Prins R. MAS NMR, TPR, and TEM Studies of the Interaction of NiMo with Alumina and Silica-Alumina Supports. *J. Catal.*, 2003, **215** (1), P. 7–13.

[19] Liu Z., Han W., Hu D., Sun S., Hu A., Wang Z., Jia Y., Zhao X., Yang Q. Effects of Ni–Al_2O_3 Interaction on NiMo/Al_2O_3 Hydrodesulfurization Catalysts. *J. Catal.*, 2020, **387**, P. 62–72.

[20] Nepomnyashchiy A.A., Buluchevskiy E.A., Lavrenov A.V., Yurpalov V.L., Gulyaeva T.I., Leont'eva N.N., Talzi V.P. Hydrodeoxygenation of Vegetable Oil on NiMoS/WO_3—Al_2O_3 Catalysts. *Russian J. of Applied Chemistry*, 2017, **90** (12), P. 1944–1952.

[21] Salomatina A.A., Nadeina K.A., Klimov O.V., Danilova I.G., Gerasimov E.Y., Prosvirin I.P., Pakharukova V.P., Chesalov Y.A., Noskov A.S. Influence of Ni/Mo Ratio on Structure Formation of Ni-Mo Complex Compounds in NiMo/Al_2O_3 Catalysts for Selective Diene Hydrogenation. *Energy and Fuels*, 2022, **36** (24), P. 15088–15099.

[22] Kordouli E., Pawelec B., Kordulis C., Lycourghiotis A., Fierro J.L.G. Hydrodeoxygenation of Phenol on Bifunctional Ni-Based Catalysts: Effects of Mo Promotion and Support. *Appl. Catal. B*, 2018, **238**, P. 147–160.

[23] Kohler S.D., Ekerdt J.G., Kim D.S., Wachs I.E. Relationship between Structure and Point of Zero Surface Charge for Molybdenum and Tungsten Oxides Supported on Alumina. *Catal. Letters*, 1992, **16**, P. 231–239.

[24] Subramanian S., Noh J.S., Schwarz J.A. Determination of the Point of Zero Charge of Composite Oxides. *J. Catal.*, 1988, **114** (2), P. 433–439.

[25] Shinkevich K.S., Kukushkin R.G., Bulavchenko O.A., Zaikina O.O., Alekseeva M.V., Ruvinskiy P.S., Yakovlev V.A. Influence of the Support on Activity and Stability of Ni and Ni-Mo Catalysts in the Hydroprocessing of Fatty Acids into Motor Fuels Components. *Appl. Catal. A Gen.*, 2022, **644**, 118801.

[26] Kovalevskaya K.S., Kukushkin R.G., Zaikina O.O., Bulavchenko O.A., Larina T.V., Golubev I.S., Yakovlev V.A. NiMo/ZSM-23 Catalysts for Deoxygenation and Isomerization of C_{16}-C_{18} Fatty Acids to Sustainable Diesel and Jet Fuel Components. *Fuel*, 2025, **383**.

[27] Sukhorukov D.A., Kukushkin R.G., Alekseeva (Bykova) M.V., Bulavchenko O.A., Zaikina O.O., Revyakin M.E., Kazakov M.O., Yakovlev V.A. Upgrading of Sewage Sludge-Derived Pyrolysis Oil via Hydrotreatment over NiMo-Based Catalysts. *Fuel*, 2024, **359**, 130383.

[28] Tobias R.S. Infrared and Raman Spectra of Inorganic and Coordination Compounds (Nakamoto, Kazuo). *J. Chem. Educ.*, 1979, **56** (5), A209.

[29] Jeziorowski H., Knözinger H. Raman and Ultraviolet Spectroscopic Characterization of Molybdena on Alumina Catalysts. *J. of Physical Chemistry*, 1979, **83** (9), P. 1166–1173.

[30] Teixeira da Silva V.L.S., Frety R., J M.S. Activation and Regeneration of a NiMo/Al_2O_3 Hydrotreatment Catalyst. *Ind. Eng. Chem. Res.*, 1994, **33**, P. 1692–1699.

[31] Guevara-Lara A., Bacaud R., Vrinat M. Highly Active NiMo/TiO_2—Al_2O_3 Catalysts: Influence of the Preparation and the Activation Conditions on the Catalytic Activity. *Appl. Catal. A Gen.*, 2007, **328** (2), P. 99–108.

[32] Vroulias D., Gkoulemani N., Papadopoulou C., Matralis H. W—Modified Ni/Al_2O_3 Catalysts for the Dry Reforming of Methane: Effect of W Loading. *Catal. Today*, 2020, **355**, P. 704–715.

[33] Priecel P., Kubička D., Čapek L., Bastl Z., Ryšánek P. The Role of Ni Species in the Deoxygenation of Rapeseed Oil over NiMo-Alumina Catalysts. *Appl. Catal. A Gen.*, 2011, **397** (1–2), P. 127–137.

[34] Arun N., Maley J., Chen N., Sammynaiken R., Hu Y., Dalai A.K. NiMo Nitride Supported on Al_2O_3 for Hydrodeoxygenation of Oleic Acid: Novel Characterization and Activity Study. *Catal. Today*, 2017, **291**, P. 153–159.

[35] Fan X., Liu D., Zhao Z., Li J., Liu J. Influence of Ni/Mo Ratio on the Structure-Performance of Ordered Mesoporous Ni–Mo–O Catalysts for Oxidative Dehydrogenation of Propane. *Catal. Today*, 2020, **339**, P. 67–78.

[36] Bankar P.K., Ratha S., More M.A., Late D.J., Rout C.S. Enhanced Field Emission Performance of $NiMoO_4$ Nanosheets by Tuning the Phase. *Appl. Surf. Sci.*, 2017, **418**, P. 270–274.

[37] Al-Dalama K., Stanislaus A. Temperature Programmed Reduction of SiO_2-Al_2O_3 Supported Ni, Mo and NiMo Catalysts Prepared with EDTA. *Thermochim. Acta*, 2011, **520** (1–2), P. 67–74.

[38] Klimov O.V., Pashigreva A.V., Bukhtiyarova G.A., Budukva S.V., Fedotov M.A., Kochubey D.I., Chesalov Y.A., Zaikovskii V.I., Noskov A.S. Bimetallic Co-Mo Complexes: A Starting Material for High Active Hydrodesulfurization Catalysts. *Catal. Today*, 2010, **150** (3–4), P. 196–206.

[39] Brito J.L., Laine J., Pratt K.C. Temperature-Programmed Reduction of Ni-Mo Oxides. *J. Mater. Sci.*, 1989, **24** (2), P. 425–431.

[40] Yang F., Libretto N.J., Komarneni M.R., Zhou W., Miller J.T., Zhu X., Resasco D.E. Enhancement of M-Cresol Hydrodeoxygenation Selectivity on Ni Catalysts by Surface Decoration of MoO_x Species. *ACS Catal.*, 2019, **9** (9), P. 7791–7800.

[41] Yang J., Zuo T., Lu J. Effect of Preparation Methods on the Hydrocracking Performance of NiMo/Al_2O_3 Catalysts. *Chin. J. Chem. Eng.*, 2021, **32**, P. 224–230.

[42] Ameen M., Azizan M.T., Ramli A., Yusup S., Alnarabiji M.S. Catalytic Hydrodeoxygenation of Rubber Seed Oil over Sonochemically Synthesized Ni-Mo/γ-Al_2O_3 Catalyst for Green Diesel Production. *Ultrason. Sonochem.*, 2019, **51**, P. 90–102.
[43] Kaddouri A., Rosso R.D., Mazzocchia C., Fumagalli D. Isotermal Reduction Behavior of Undoped and Ca-, K- Nd P-Doped $NiMoO_4$ Phases Used for Selective Propane Oxydehydrogenation. *J. Therm. Anal. Calorim.*, 2001, **63**, P. 267–277.
[44] Chen M., Wu J.L., Liu Y.M., Cao Y., Guo L., He H.Y., Fan K.N. A Practical Grinding-Assisted Dry Synthesis of Nanocrystalline $NiMoO_4$ Polymorphs for Oxidative Dehydrogenation of Propane. *J. Solid State Chem.*, 2011, **184** (12), P. 3357–3363.
[45] Plyasova L.M., Ivanchenko I.Y., Andrushkevich M.M., Buyanov R.A., Itenberg I.S., Khramova G.A., Karakchiev L.G., Kustova G.N., Stepanov G.A., Tsailingol'd A.L., Pilipenko F.S. Study of the Phase Composition of Nickel-Molybdenum Catalysts. *Kinetics and Catalysis*, 1973, **14** (4), P. 882–886.
[46] Chen Y., Li C., Chen X., Liu Y., Liang C. Synthesis of ZSM-23 Zeolite with Dual Structure Directing Agents for Hydroisomerization of n-Hexadecane. *Microporous and Mesoporous Materials*, 2018, **268**, P. 216–224.
[47] Bai D., Meng J.P., Zou C., Li C., Liang C. H. Manipulation of Hydroisomerization Performance on Pt/ZSM-23 by Introducing Al_2O_3. *Journal of Fuel Chemistry and Technology*, 2023, **51** (2), P. 175–185.
[48] Wang Q., Sim L.B., Xie J., Ye S., Fu J., Wang J., Zhang N., Zheng J., Chen B. Comparative Study of Pt/Zeolites for n-Hexadecane Hydroisomerization: EU-1, ZSM-48, ZSM-23, ZSM-22, and ZSM-12. *Chem. Eng. Sci.*, 2024, **287**, 119785.
[49] Ding S., Li F., Li Z., Yu H., Song C., Xiong D., Lin H. Catalytic Hydrodeoxygenation of Waste Cooking Oil and Stearic Acid over Reduced Nickel-Based Catalysts. *Catal. Commun.*, 2021, **149**, 106235.
[50] Wang Z., Jia X., Yan Z., Fu W., Li Z., Tang T., Zhang L. CrOx Modified Particles Size and Electronic Density of Ni Catalyst on ZSM-23 for Enhanced Hydroisomerization Performance of Long-Chain n-Alkanes. *Fuel*, 2024, **367**, 131476.
[51] Tu C., Chen J., Li W., Wang H., Deng K., Vinokurov V.A., Huang W. Hydrodeoxygenation of Bio-Derived Anisole to Cyclohexane over Bi-Functional IM-5 Zeolite Supported Ni Catalysts. *Sustain. Energy Fuels*, 2019, **3** (12), P. 3462–3472.
[52] Mannei E., Ayari F., Petitto C., Asedegbega-Nieto E., Guerrero-Ruiz A. R., Delahay G., Mhamdi M., Ghorbel A. Light Hydrocarbons Ammoxidation into Acetonitrile over Mo—ZSM-5 Catalysts: Effect of Molybdenum Precursor. *Microporous and Mesoporous Materials*, 2017, **241**, P. 246–257.
[53] Wang J., Chen Y., Liu C., Lu Y., Lin X., Hou D., Luo C., Wang D., Zheng Z., Zheng Y. Highly Stable Mo-Based Bimetallic Catalysts for Selective Deoxygenation of Oleic Acid to Fuel-like Hydrocarbons. *J. Environ. Chem. Eng.*, 2023, **11** (1), 109104.
[54] Bal'zhinimaev B.S., Paukshtis E.A., Suknev A.P., Makolkin N.V. Highly Selective/Enantioselective Pt-ReOx/C Catalyst for Hydrogenation of L-Malic Acid at Mild Conditions. *J. of Energy Chemistry*, 2018, **27** (3), P. 903–912.
[55] Alvarez F., Ribeiro F.R., Perot G., Thomazeau C., Guisnet M. Hydroisomerization and Hydrocracking of Alkanes. 7. Influence of the Balance between Acid and Hydrogenating Functions on the Transformation of n-Decane on PtHY Catalysts. *J. Catal.*, 1996, **162** (2), P. 179–189.
[56] Gosselink R.W., Hollak S.A.W., Chang S.W., Van Haveren J., De Jong K.P., Bitter J.H., Van Es D.S. Reaction Pathways for the Deoxygenation of Vegetable Oils and Related Model Compounds. *Chem. Sus. Chem.*, 2013, **6** (9), P. 1576–1594.
[57] Bourikas K., Kordulis C., Lycourghiotis A. The Role of the Liquid-Solid Interface in the Preparation of Supported Catalysts. *Catal. Rev. Sci. Eng.*, 2006, **48** (4), P. 363–444.
[58] Fedyna M., Żak A., Jaroszewska K., Mokrzycki J., Trawczyński J. Composite of Pt/AlSBA-15+zeolite Catalyst for the Hydroisomerization of n-Hexadecane: The Effect of Platinum Precursor. *Microporous and Mesoporous Materials*, 2020, **305** (May).
[59] Knyazheva O.A., Baklanova O.N., Lavrenov A.V., Buluchevskii E.A., Drozdov V.A., Trenikhin M.V., Leont'eva N.N., Vasilevich A.V., Likholobov V.A. Mechanochemical Synthesis of Nanocrystalline Nickel—Molybdenum Compounds and Their Morphology and Application in Catalysis: III. Catalytic Properties of Massive Ni–Mo Sulfide Catalysts Synthesized Using Mechanochemical Activation. *Kinetics and Catalysis*, 2014, **55** (1), P. 130–138.
[60] Knyazheva O.A., Baklanova O.N., Lavrenov A.V., Buluchevskii E.A., Gulyaeva T.I., Leont'eva N.N., Drozdov V.A., Likholobov V.A., Vasilevich A.V. Mechanochemical Synthesis of β-$NiMoO_4$ as a Precursor of Bulk Highly Dispersed Catalyst for the Hydrocracking of Oil Fractions. *Catalysis in Industry*, 2012, **4** (3), P. 179–185.
[61] Nepomnyashchiy A.A., Saibulina E.R., Buluchevskiy E.A., Gulyaeva T.I., Yurpalov V.L., Mironenko R.M., Potapenko O.V., Lavrenov A.V. Combined Deoxygenation and Isomerization of Sunflower Oil Fat Acid Triglycerides on Pt/Al_2O_3-Zeolite Catalysts. *Catalysis in Industry*, 2024, **16** (2), P. 170–177.
[62] Nepomnyashchiy A.A., Yurpalov V.L., Buluchevskiy E.A., Drozdov V.A., Gulyaeva T.I., Mironenko R.M., Lavrenov A.V. Hydrodeoxygenation of Sunflower Oil on Pt/WO_x-Al_2O_3 Catalyst. *Catalysis in Industry*, 2024, **16** (2), P. 187–195.

Submitted 23 May 2025; revised 21 October 2025; accepted 15 November 2025

Information about the authors:

Ksenia S. Kovalevskaya – Boreskov Institute of Catalysis SB RAS, Akademika Lavrentieva av. 5, 630090, Novosibirsk, Russia; ORCID 0000-0003-3558-4918; shinkevich@catalysis.ru

Roman G. Kukushkin – Boreskov Institute of Catalysis SB RAS, Akademika Lavrentieva av. 5, 630090, Novosibirsk, Russia; ORCID 0000-0001-8124-352X; roman@catalysis.ru

Olesya O. Zaikina – Boreskov Institute of Catalysis SB RAS, Akademika Lavrentieva av. 5, 630090, Novosibirsk, Russia; omironenko@catalysis.ru

Olga A. Bulavchenko – Boreskov Institute of Catalysis SB RAS, Akademika Lavrentieva av. 5, 630090, Novosibirsk, Russia; ORCID 0000-0001-5944-2629; isizy@catalysis.ru

Vadim A. Yakovlev – Boreskov Institute of Catalysis SB RAS, Akademika Lavrentieva av. 5, 630090, Novosibirsk, Russia; ORCID 0000-0001-5015-3521; yakovlev@catalysis.ru

Conflict of interest: the authors declare no conflict of interest.